# Silk and Silk Composite Aerogel Based Biocompatible Triboelectric Nanogenerators for Efficient Energy Harvesting

*Hao-Yang Mi[a,b]\*, Heng Li[c], Xin Jing[b]\*, Ping He[e], Pei-Yong Feng[b], Xiaoming Tao[d], Yuejun Liu[b], Chuntai Liu[a], Changyu Shen[a]*

[a] Key Laboratory of Materials Processing and Mold, Zhengzhou University, Zhengzhou, 450000, China

[b] Key Laboratory of Advanced Packaging Materials and Technology of Hunan Province, Hunan University of Technology, Zhuzhou, 412007, China

[c] Department of Building and Real Estate, Hong Kong Polytechnic University, Hong Kong, 518000, China

[d] Institute of Textile and Clothing, Hong Kong Polytechnic University, Hong Kong, 999077, China

[e] Department of Industrial Engineering, Jinan University, Zhuhai, Guangdong, 519070, China.

**Corresponding Authors:**

H.Y. Mi  E-mail: mihaoyang@zzu.edu.cn
X. Jing  E-mail: jingxinscut@gmail.com

Note:

The authors declare no competing financial interest.

**Abstract:**

Triboelectric nanogenerators (TENGs) with high performance and biocompatibility are of the demand for the development of novel medical devices and wearable electronics. Herein, a highly porous silk aerogel based TENG (STENG) with high output performance was developed using silk fibroin extracted from silk cocoon. The silk aerogel made of 2 % silk fibroin solution showed a nano fibrillated porous structure and the highest surface area, which contributed to the high triboelectric output performance of the STENG based on it. The rough surface and highly porous structure facilitated charge generation of the aerogels. The optimized STENG achieved an open circuit voltage of 52.8 V and short circuit current of 5.2 μA, and a maximum power density of 0.37 W/m$^2$ was reached on a 1 MΩ external resistor. The STENG possesses high stability under different operation frequency and in long term, and it could act as a power source for small electronics. Moreover, the excellent biocompatibility of silk aerogels to human cells makes the STENG possible as implantable energy harvesters. In addition, due to its high tribopositivity, silk can be used as additives to fabricate composite aerogel. With addition of 20 % silk, the power of cellulose nanofibril (CNF) based TENG improved by 3.1 times.

**Keywords:** Triboelectric nanogenerator; silk; aerogel; biocompatible; silk composite

# 1. Introduction

Energy crisis and environmental problems caused by traditional fuel based thermal power generation are critical challenges for human beings in the twenty first century. Searching for alternative green and sustainable energy sources is becoming a more and more important global topic. [1, 2] Harvesting energy from wind, water potential, and sunlight have been researched for decades and widely used in many countries. [3] In recent decade, more and more researchers are devoting to techniques that harvest mechanical energy in nature and people's daily life, which probably is the most widely existed and wasted energy source. [4, 5] Among all current developed mechanical energy harvesting technologies, triboelectric nanogenerators (TENGs) have the unique advantage of capable to harvest chaotic mechanical energy from human daily life and nature. [6-8] So far, TENGs have been successfully used to harvest mechanical energy in various circumstances, such as machine vibration, wheel rotation, human motion, wind, and ocean waves, [9-14] and also find their applications in sound recording, angle measurement, motion sensing, traffic volume and even biomedical field. [15-18] Developing TENGs with biocompatibility, biodegradability, and bioabsorbability is of the demand for medical devices, and tissue repairing applications. [19]

TENG generates energy by the coupling effect of contact electrification and electrostatic induction. [20] The amount of charges generated upon the contact of tribopositive and tribonegative materials greatly affects the energy output of a TENG device. [21, 22] Generally, two dissimilar materials with opposite tribopolarity would generate opposite charges on them when they are in contact. [23, 24] Developing new biocompatible triboelectric materials with high tribopolarity is important for boosting output performance and extending application of TENGs in biomedical fields. [25] Triboelectric series ranks various materials based on their tribopolarity, and the ones ranked at the bottom of the triboelectric series have high tribonegativity. [26] Polydimethylsiloxane (PDMS) and polytetrafluoroethylene (PTFE) are

ideal tribonegative materials for biocompatible TENGs. They are highly biocompatible and have been widely used in many medical devices. [27, 28] However, tribopositive materials with high biocompatibility are rarely investigated. Kim et al. developed a new butylated melamine formaldehyde polymer as highly durable tribopositive material. [29] Wu et al. recently reported a chitosan based TENG that capable to be used as biocompatible TENG, but its output performance was fairly low with output current in nA range. [30]

Searching from the top of the triboelectric series, silk probably is the most favorable biocompatible material with high tribopositivity. [31] Excellent biocompatibility and bioabsorbability of silk make it possible to be used in implantable electronics. [32, 33] Oh et al. developed the first electrospun silk fiber based TENG in 2016, but it had a relatively low power density of 4.3 mW/m$^2$. [34] Wang et al. recently developed a series of nature material based TENGs. Among them, silk fibroin based TENG showed superior output performance than other TENGs based on cellulose and chitin. The maximum power density achieved with optimized combination was 21.6 mW/m$^2$. [33] He et al. developed a silk based hydrogel by combining with polyacrylamide, graphene oxide, and poly(3,4-ethylenedioxythiophene): poly(styrenesulfonate). The hydrogel could serve as a single electrode TENG due to tribopositivity of silk. [35] Wen et al. fabricated a multi-functional sensor that is composed of PDMS, printed graphene electrode and silk fibroin film. The sensor could detect water molecules and generates power by contact with human skin. However, the TENG function was mainly supplied by the PDMS layer. [36] So far, silk based TENGs are rarely reported and performance are usually low, so we believe there is still a large room to improve their performance, and it would be highly valuable for the development of biocompatible TENG.

Surface engineering is a frequently used approach to boost TENG output by enriching the surface topography of triboelectric materials and increase the surface area, which would induce more charge generation by providing more contact surfaces. [37] However, surface engineering is a delicate and high cost approach that might be improper for bio-based

4

materials and unpractical for mass production. Aerogels, as a rising star material in this century, have attracted tremendous attentions due to their super light-weight, high surface area, excellent barrier properties, ease of fabrication, and low cost. [38] Recent studies have verified the capability of highly porous aerogel based membranes as triboelectric layers in TENG fabrication, and confirmed remarkable improvement in triboelectric output when solid films are replaced with aerogels in various TENGs. The advantages of porous aerogel are their porous structure exposed on material surface which endows high surface area, and the interconnected inner pores which would induce charge generation in the inner parts of the aerogel membrane. [39, 40]

Aiming to develop a novel biocompatible TENG with high performance, a series of silk fibroin aerogels were fabricated by freeze-drying and used to fabricate silk based TENGs (STENGs) in this study. The effect of aerogel property on the STENG performance was investigated comprehensively in order to understand the underlying mechanism and optimize STENG performance. The maximum output voltage of 52.8 V and output current of 5.2 μA were achieved on the STENG composed of silk aerogel that has the greatest surface area. An optimum power density of 0.37 W/m$^2$ was achieved on a 1 MΩ resistor. Moreover, silk fibroin can be used as additive material to enhance the triboelectric output of cellulose nanofibrils (CNF) aerogel based TENG due to its high tribopositivity. The developed STENG also possesses high long term stability and capability to be used as power source for small electronics.

## 2. Experimental Methods

### 2.1 Preparation of silk fibroin solution

Silk fibroin was extracted from raw silk fibers following our previous work. Briefly, silk fiber membrane from nature bombyx mori was boiled in a 0.02 M Na$_2$CO$_3$ aqueous

solution for 30 min with manual stirring. Then the dispersed silk fibers were rinsed with DI water three times to remove the glue-like silk sericin followed by drying at room temperature for 2 days. To prepare the silk fibroin solution, 5 g dried silk fibers were dissolved in 20 mL 9.3 M LiBr solution completely at 60 °C for 4 h with magnetic stirring. Then, the solution was dialyzed in DI water for 3 days at room temperature using cellulose membrane (MWCO 14,000, Sigma-Aldrich). The DI water was replaced every 6 to 8 hours to remove LiBr. The impurities in the obtained solution were removed by centrifugation at 10,000 rpm for 40 min at 4 °C. The concentration of silk fibroin was calculated by measuring the weight of 1 mL freeze dried solution. It usually has a concentration of 6 to 8 % in water.

*2.2 Preparation of silk fibroin aerogel*

The silk fibroin solution was diluted using DI water to prepare solutions with silk fibroin concentration of 1 %, 2%, and 4%. 5 mL different solutions were poured into aluminium dishes and cooled to 4 °C for 1 h. Then, the solutions were frozen in acetone/dry ice bath for 10 min and in –20 °C freezer for 1 h, followed by freeze drying at –84 °C for 3 days using a freeze dryer (Labconco).

*2.3 Fabrication of silk fibroin aerogel based triboelectric nanogenerator (STENG)*

The obtained aerogels were compressed into thin films with thickness of 0.2 mm using a mechanical property test instrument (Instron) at a crosshead speed of 1 mm/min and holded for 10 min. The obtained silk aerogel films were cut into rectangular pieces (2 cm × 1 cm) and attached to indium tin oxide (ITO)-coated flexible polyethylene terephthalate (PET) (ITO/PET) films to be used as the tribopositive layer. The tribonegative layer was fabricated in the same approach by attaching PTFE filter paper on ITO/PET film. Then, the two layers were separated using two PDMS spacers with a thickness of 2.5 mm. Aluminum strands were attached on ITO/PET films in order to connect to external circuit.

*2.4 HEF1 Human Fibroblasts Culture*

HEF1 fibroblast cells differentiated from the human embryonic stem cell line WA09 (WiCell Research Institute) were used for the cell culture studies on the prepared aerogel films. The cells were cultured in a medium comprised of 80% knockout Dulbecco's modified Eagle's medium (KO-DMEM) (Invitrogen, Carlsbad, CA), 1 mM L-glutamine, 0.1 mM b-mercaptoethanol, 20% fetal bovine serum (FBS) (Hyclone, Logan, UT), and 1% non-essential amino acids. The outgrowth culture was passaged by incubation in TrypLE (Invitrogen) for 5 min. Prior to cell seeding, samples were rinsed with PBS for 3 times and then sterilized with ultraviolet (UV) light for 30 min each side. HEF1 cells were seeded onto the aerogel films at a density of $1 \times 10^4$ cells per well and cultured in an incubator with 5% $CO_2$ at 37 °C. Cells were fed with HEF1 media every two days.

*2.5 Characterization of materials and TENGs*

The morphology of specimens was imaged using a scanning electron microscope (SEM, LEO GEMINI 1530, Zeiss) at an acceleration voltage of 3 kV. All samples were sputtered with a thin film of gold before imaging. The porosity of the PI aerogel was calculated by $P = (1 - \rho_b / \rho_d) \times 100\%$, where $\rho_b$ was the bulk density and $\rho_d$ was the density of the solid material. The Brunauer–Emmett–Teller (BET) surface area of the PA nanofiber mats and the PI aerogel films were measured by $N_2$ physisorption using a Gemini VII 2390 surface area analyzer (Micromeritics Instrument Corp.). All statistical measurements were performed at least in triplicate. Mechanical property was tested on a universal mechanical tester (instron). Samples were cut into $5 \times 1$ cm pieces and stretched at a crosshead speed of 1 mm/min until fracture. A home-made setup consisting of a dynamic shaker (Shiao, SA-JZ), a signal generator (BK Precision, 4003A) and a signal amplifier (Yamaha, A-S201) was used to evaluate the triboelectric output performance of the TENGs. The open circuit voltage signal generated was recorded using an oscilloscope (ZDS3034 Plus) and the short circuit current signal was recorded using a potentiostat (CHI760E). The power density on specific resistor

was calculated using $PD = I^2R/A$, where I was the peak current, A was the contact area of the TENG, and R was the resistance of external load. All tests were performed at least three times, and the most representative curves were reported.

*2.6 Characterization of Biological Properties*

Cell viability was determined after culturing for 7 and 14 days. Viability was assessed via a live/dead viability/cytotoxicity kit. Green fluorescent calcein-AM was used to target esterase activity within the cytoplasm of living cells, while red fluorescence ethidium homodimer-1(EthD-1) was used to indicate cell death. Stained cells were imaged with a Nikon A1RSi inverted confocal microscope system. Cell proliferation was assessed by MTS assay using the CellTiter 96 Aqueous One Solution kit (Promega Life Sciences). Cells were first treated with media containing a 20% MTS solution and allowed to incubate for 1 h. After incubation, 100 µL of spent media were transferred into a clear 96-well plate. The absorbance of the plates at the 450 nm wavelength was read with a Glomax-Multi+Multiplate Reader (Promega). The subsequent number of cells was determined relative to the negative control.

## 3. Results and Discussion

Figure 1a depicts the structure of the developed STENG. Raw silk or silk aerogel was used as tribropositive layer due to their high tribopositivity, PTFE filter paper was used as tribronegative layer because of its high porosity and tribonegativity. The triboelectric materials were attached on two ITO coated PET (ITO/PET) sheets which were separated using two PDMS spacers, so that the STENG can operated in a contact-separation mode. Figure 1 b shows the morphology of PTFE filter paper, it has a highly porous structure with average pore size about 200 nm. Silk fiber membrane was directly obtained from silk cocoon as shown in Figure 1c and d. The raw silk fibers showed a nonwoven structure with average diameter of ~6 µm. The morphology of silk fibroin aerogels fabricated with different solution

concentrations was shown in Figure 1e-g. It was noticed that the silk fibroin solution concentration had a significant influence on the aerogel morphology. At low concentration (1 %), silk aerogel showed a porous structure with film-like pore walls, and the pores are generally in few micrometers range (Figure 1e). At 2 % concentration, the pores of silk aerogel were much smaller and more uniform compared to the 1 % silk aerogel as shown in Figure 1f. The surface of 2 % aerogel is mainly composed of nano sized fibril-like structure and sub-micro sized pores. However, when the concentration is further increased to 4 %, nano fibrils started to merge together into films and some pores were cover by the films, which reduced the textures on aerogel surface.
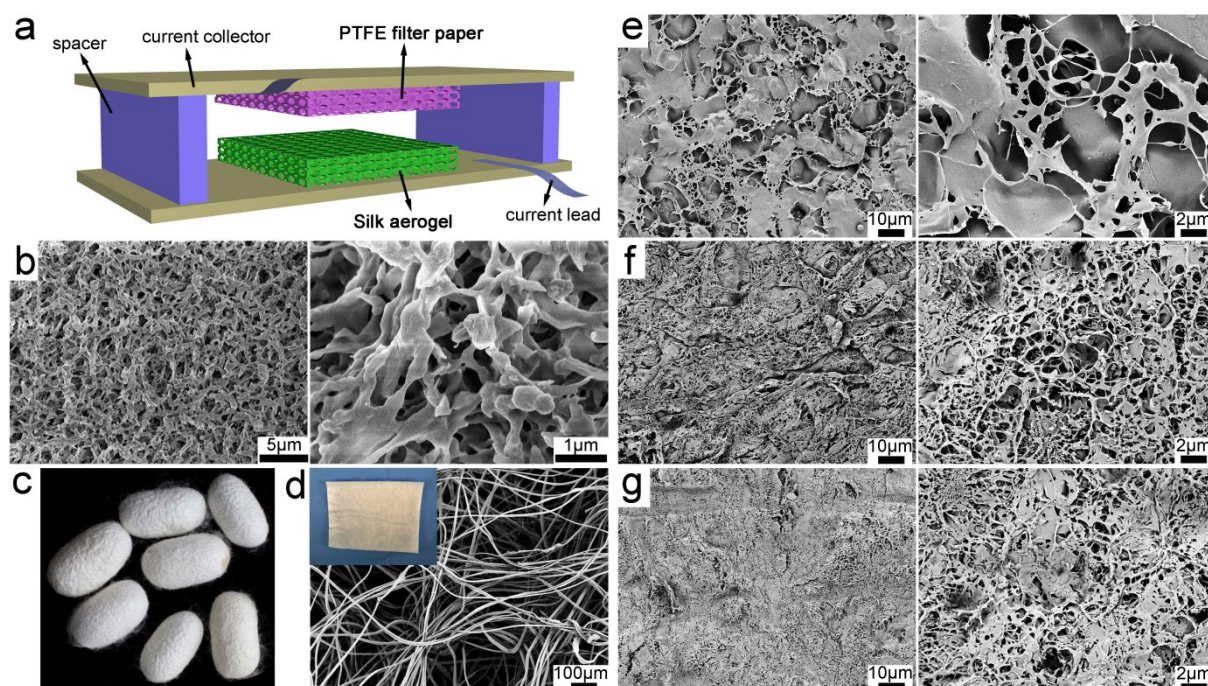


**Figure 1.** (a) Schematic illustration of the structure of STENG; (b) SEM images of PTFE filter paper; (c) Photograph of silk cocoon; (d) SEM image of raw silk fibers, inset shows the raw silk membrane; SEM images of silk aerogels prepared using silk fibroin solutions with concentration of (e) 1 %, (f) 2 %, and (g) 4 %.

The bulk property of silk fiber and silk aerogel was measured to investigate the major governing factors of porous materials affecting their triboelectric output performance. As

shown in Figure 2a, the bulk density of raw silk fiber membrane was the lowest (0.18 g/cm$^3$) due to its fluffy structure. The bulk density increased from 0.37 to 0.6 g/cm$^3$ as the increase of solution concentration for the silk aerogels. The porosity, on the contrary, showed an opposite trend. As shown in Figure 2b, the raw silk fiber had the highest porosity of 86.6 %, while the 4 % silk aerogel showed the lowest porosity of 55.4 %. Interestingly, the surface area of raw silk fiber (1.4 m$^2$/g) was significantly lower than all silk aerogels, while the 2 % silk aerogel had the highest surface area of 18.5 m$^2$/g. The surface area of materials is highly related to their microstructures. According to Figure 1, the 2 % silk aerogel showed the optimum porous structure consisting of submicro pores and nano fibrils. It also had the minimum film formation compared to other silk aerogels. However, the raw silk fiber has a fiber diameter in micro scale and the pores are generally greater than 100 μm, which was the reason for its low surface area. The tensile test results showed that the silk fiber membrane had the lowest tensile strength and modulus as shown in Figure S1. The tensile strength, modulus, and elongation-at-break all increased as the increase of silk concentration for the silk aerogels. The 1 % silk aerogel film exhibited a fragile feature with elongation-at-break about 1 % indicating brittleness behavior. The elongation-at-break increased to over 3 % for the 2 % silk aerogel, and over 10 % for the 4% silk aerogel suggesting the improvement of material flexibility.
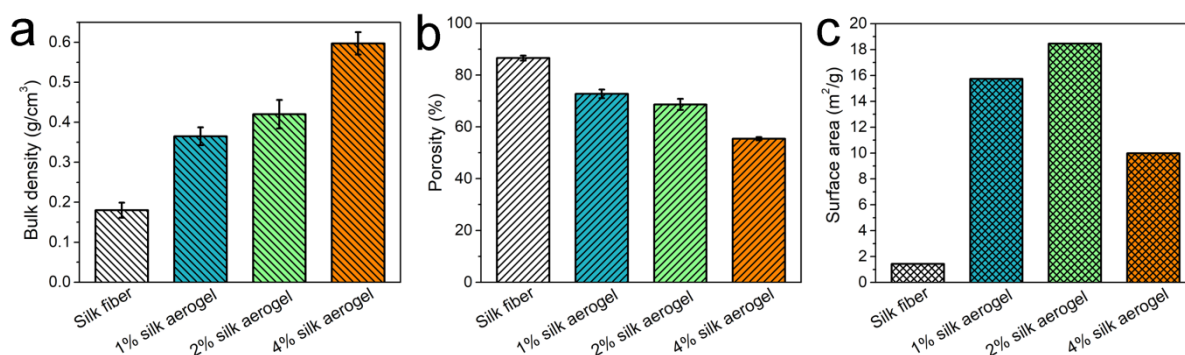


**Figure 2.** (a) Bulk density, (b) porosity, and (c) surface area of raw silk fiber membrane and silk aerogels with concentration of 1 %, 2%, and 4 %.

To verify the biocompatibility of silk fiber and silk aerogel, they were seeded with HEF1 human fibroblast cells for up to 14 days. From the fluorescent images (Figure 3a), the cells were able to attach and proliferate on both silk fiber membrane and silk aerogel. Most cells on the samples are live cells and are uniformly distributed across the whole sample surface. The statistical results of live/dead assay (Figure 3b) indicated that both samples had average cell viability over 90 % at both day 7 and day 14 time points, which were higher than the control group on TCP. The statistical results of MTS assay (Figure 3c) indicated that the cell population on silk aerogel was significantly greater than both silk fiber and TCP at both day 7 and day 14. The higher cell population on silk aerogel might be attributed to greater surface area and better biocompatibility of extracted silk fibroin than raw silk fibers. [41] However, the fibroblast cells on silk fiber membrane showed larger cell size and more elongated cell morphology than the cells on silk aerogel (Figure S2), because the silk fiber provided an elongated substrate that is more favorable for cell alignment. [42] Nevertheless, the cell culture results confirmed that both materials possess high biocompatibility to human fibroblasts.
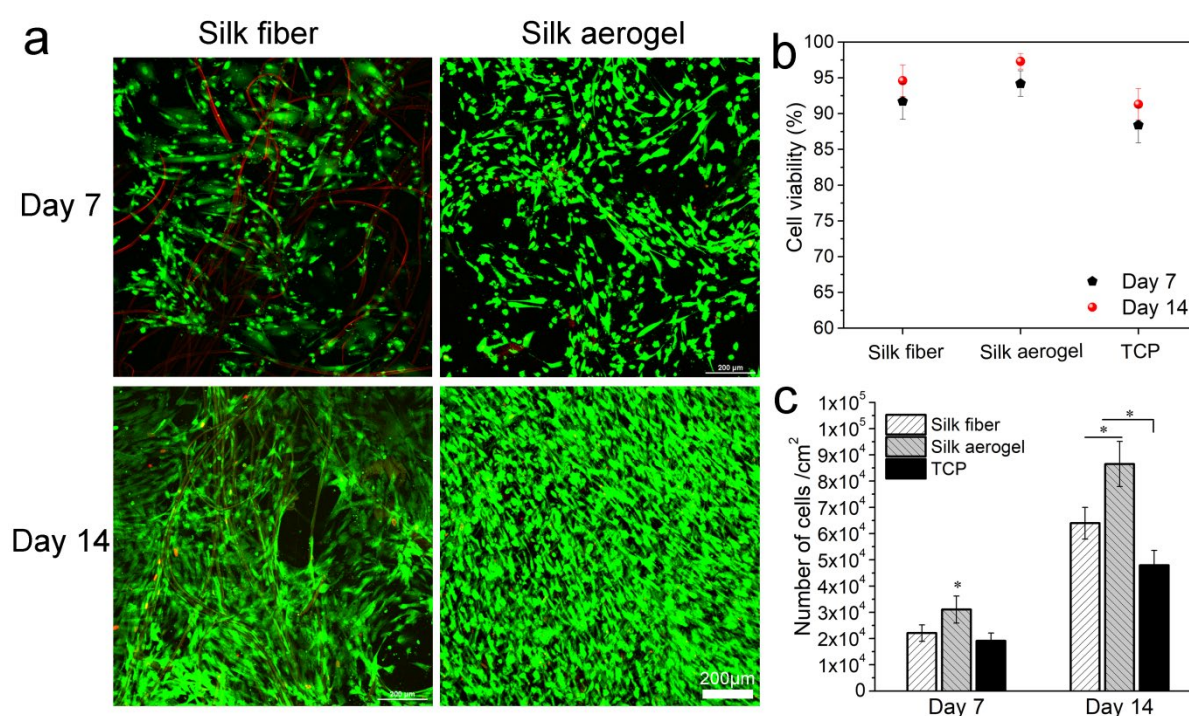
**Figure 3.** Day 7 and Day 14 results of human fibroblast cells cultured on silk fiber and silk aerogel (a) fluorescent images of live/dead assay with green color indicates live cell and red color indicates dead cell, (b) cell viability data from live/dead assay, (c) cell proliferation data from MTS assay.

Next, we focused on investigating the triboelectric performance of the developed STENG. Figure 4a shows the working principle of the STENG which is composed of triboelectric materials with high porosity. The STENG operates in contact-separation mode, and charges are generated when the PTFE layer is in contact with the silk layer due to the synergetic effects of contact electrification and electrostatic induction caused by the significant triboelectric property difference between PTFE and silk. [26] When the two layers are separating, a potential difference is created between the bottom and top layer, which further induced electron flow in the external circuit to compensate the potential difference until an equilibrium state is achieved. When the two layers are moving towards each other again, the electrons were pushed back in the opposite direction since the potential difference on PTFE and silk layers are compensated by each other. Thus, a positive and a negative instant current flow are generated in one pressing-releasing cycle; and mechanical energy from STENG motion is transfer to electrical energy.

The triboelectric output voltage results are shown in Figure 4b-e. It was found that STENGs made of silk aerogels had significant higher voltage than the STENG made of raw silk fiber. The instant peak voltage of STENGs made of 1 %, 2 %, and 4 % silk aerogels are 39.2 V, 52.8 V, and 30.4 V, respectively. Figure 4f-i shows the results of triboelectric output current results which exhibited the same trend with the voltage results. The instant peak current of STENGs made of 1 %, 2 %, and 4 % silk aerogels are 3.9 µA, 5.2 µA, and 3.0 µA, respectively. It was found that the STENG made of 2 % silk aerogel had the best output performance among all STENGs fabricated. The tiny peaks appeared in between adjacent

voltage and current peaks were believed to be caused by the small vibration of the TENG after each compression cycle. Considering the physical properties of the STENGs, it is believed that the surface area may play a pivotal role affecting the STENG output. Owing to the porous structure of triboelectric materials, charges are created not only on material surface, but also on the inner pores surfaces that are close to the material surface as depicted in Figure 4a. [43] With high surface area and rough surface structure, 2 % silk aerogel based STENG could generate more charges on the triboelectric layers than the other STENGs, which lead to greater output performance. Therefore, the STENG based on 2% silk aerogel is used for further investigation of STENG as power source, and its performance stability.
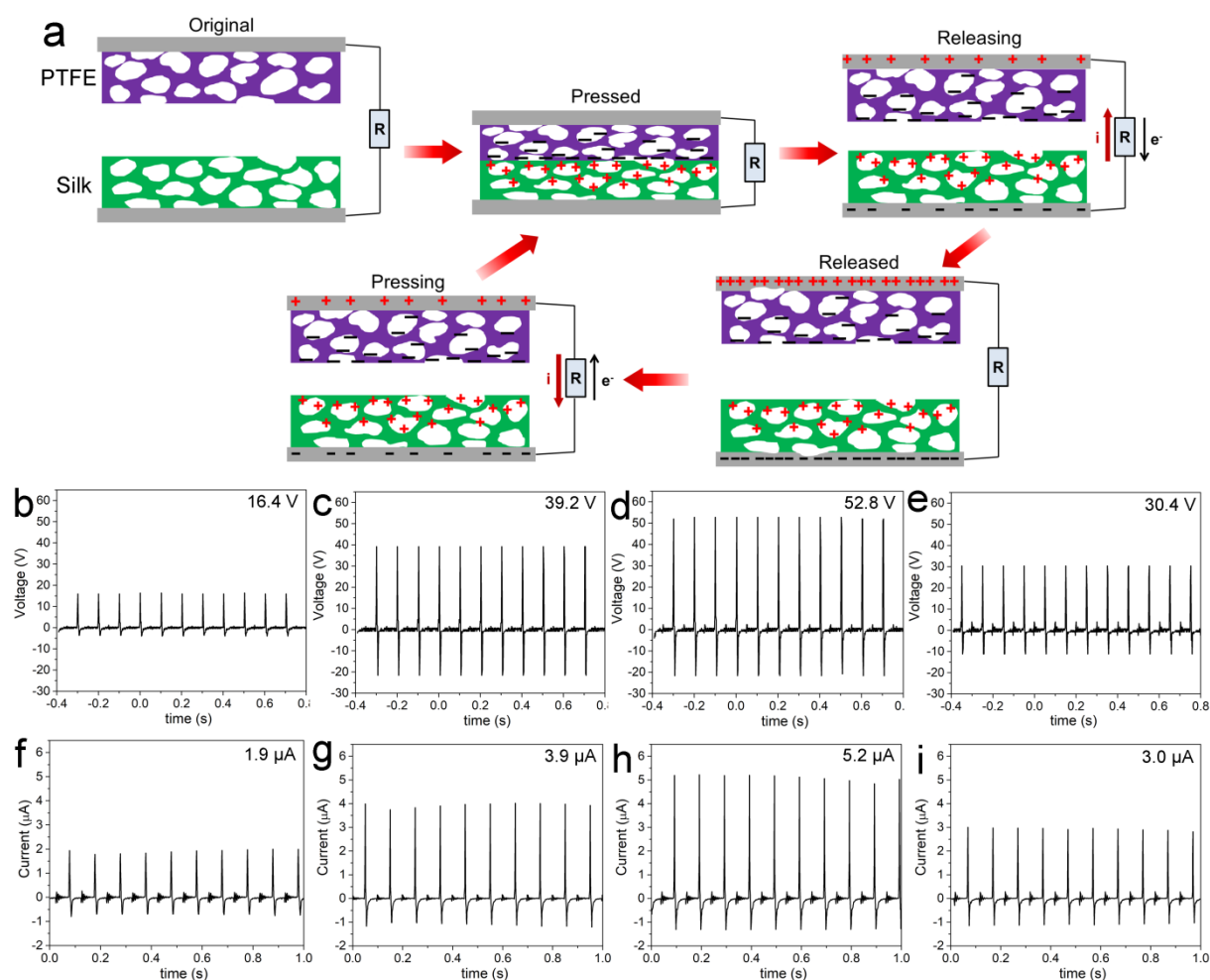


**Figure 4.** (a) Illustration of working principle of the porous STENG; Representative triboelectric output voltage results of (b) silk fiber, (c) 1% silk aerogel, (d) 2% silk aerogel, (e)

4% silk aerogel; Triboelectric output current results of (b) silk fiber, (c) 1% silk aerogel, (d) 2% silk aerogel, (e) 4% silk aerogel.


The STENG developed has small unit size and high flexibility (Figure 5a), which make it adaptable to different substrates and capable to be integrated into wearable device. To investigate the stability of the STENG, it was compressed at different frequencies ranging from 2 Hz to 10 Hz. As shown in Figure 5b, the STENG showed stable output under different frequencies. Figure 5c shows the output voltage of STENG when continuous operating for 40 min. It was found no obvious voltage reduction was observed indicating the high stability of the STENG. The long term performance of STENG was investigated by measuring its performance over 10 weeks. As shown in Figure S3, the STENG maintained about the same output voltage during 10 weeks indicating high long-term stability. Moreover, the performance of the STENG at different humidity was investigated. It was found that the output voltage decreased from 52 V to 33 V as the increase of humidity from ~40 % to ~80 % since contact electrification is more significant in dry air (Figure S4). Next, we directly used the STENG as a power source to light LEDs. As shown in Figure 5d and Movie 1, thanks to the high instant output voltage of the STENG, it could simultaneously light 28 white, blue, and green LEDs. The output power of the STENG on external load was investigated by connecting the STENG to various resistors with different resistances, and the current flow through the resistor was measured. As shown in Figure 5e, the current density was gradually decreased from 22.4 $\mu A/cm^2$ to 2.5 $\mu A/cm^2$ as the external resistance increased from 1 k$\Omega$ to 10M$\Omega$. The power density was increased at low resistance and decrease at high resistance with a maximum power density of 0.37 $W/m^2$ achieved on a 1 M$\Omega$ resistor. Since STENG generates discontinuous alternative current flow during operation, it is difficult to be directly used as a power source. In order to take use of the energy generated by the STENG, it was connected to a capacitor through a bridge rectifier which could convert the alternative current

14

flow from STENG to the same direction. Figure 5f shows the performance of the STENG to charge capacitors with different capacitances. The STENG was able to charge capacitors with capacitance of 6.8 µF, 10 µF, and 22 µF to 5 V in 202 s, 288 s, and 598 s, respectively. By using a bridge rectifier and a capacitor, the discontinuous alternative current from STENG is converted to direct current, and can be used as power source for small electronics. As demonstrated in Figure 5g and movie 2, a 10 µF capacitor charged to 7V by the STENG was able to light two purple LEDs for 2 s. The charged capacitor could also be used to power a digital timer as shown in Figure 5h and movie 3. However, the energy generated only powered the timer for about 3 s, and the energy generation rate by the STENG was not fast enough to compensate the energy consumption by the timer since the contact area of the fabricated STENG was only 2 cm$^2$. Nevertheless, we have demonstrated the potential ability of the STENG as a biocompatible green energy source.
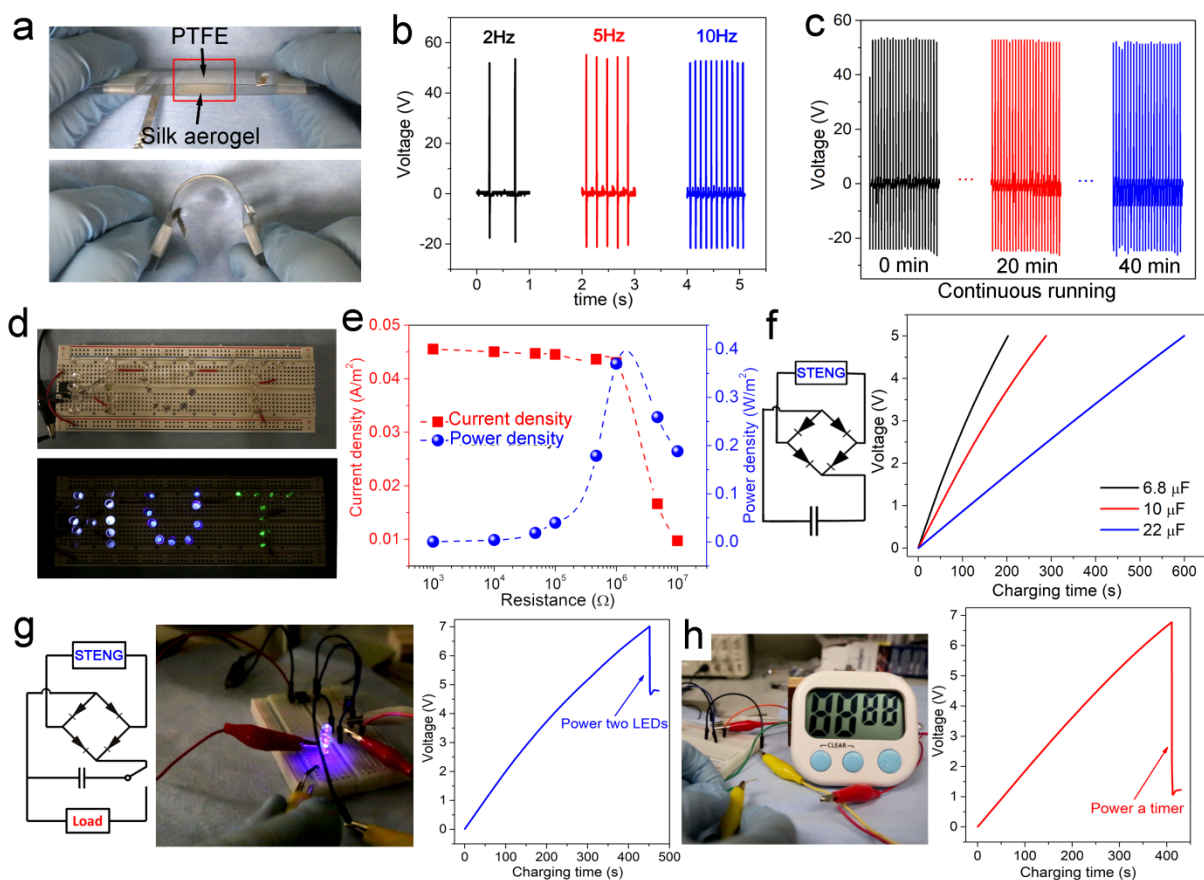
**Figure 5.** (a) Digital photograph of STENG showing high flexibility; (b) Output voltage of STENG operated at different frequency; (c) Output voltage of STENG in continuous running for 40 min; (d) Lighting LEDs using the STENG; (e) Voltage and power density of STENG on external load; (f) Charge capacitors with different capacitance using STENG; (g) Light two LEDs using a 10 μF capacitor charged by STENG; (h) Power a digital timer using a 10 μF capacitor charged by STENG.

Considering relative high cost of silk, we are interested to investigate whether silk fibroin can be used as an additive material to enhance the triboelectric performance of other low cost nature materials, such as cellulose, because silk has a high ranking in the triboelectric series. [31] Cellulose nanofibrils (CNF) is a extract from nature wood, and is a highly recognized renewable nano material. CNF aqueous solution with concentration of 1 % was prepared according to our previous procedure. [39] We have verified that the biocompatibility of CNF aerogel to human fibroblast cells in our previous work. [44] A 1% CNF/silk solution was prepared by mixing 1% silk fibroin solution with 1% CNF solution at 1 to 4 ratio, so that the mixture solution has 20 % silk and 80 % CNF. Then the solution was fabricated into CNF/silk aerogel membrane and assembled into TENG device in the same way described in the Experimental section. A TENG made of neat CNF aerogel membrane was prepared for comparison. It was found that the CNF aerogel presented superior tensile property than the silk aerogel, and the tensile properties of CNF/silk aerogels were increased as the increase of CNF content in the hybrid aerogel (Figure S5). Figure 6a and b shows the surface morphology of the CNF aerogel and CNF/silk aerogel membranes. From the inset of Figure 6a, it was found that CNF aerogel generally formed a nanofibrillated porous structure with nano sized CNF fibers uniformly distributed, while some area of the surface showed defects of large pores and groves (Figure 6a). Surprisingly, the CNF/silk aerogel exhibited a more complex surface structure compared to the CNF aerogel as shown in Figure 6b. Besides nanofibrillated

structure, some area of the CNF/silk aerogel showed film or ribbon-like structure in submicro or micrometer scale. Referring Figure 1, these structures might be attributed to the silk content in the CNF/silk composite aerogel. The physical property measurements indicated that the bulk density of CNF aerogel (0.18 g/cm$^3$) was lower than the CNF/silk aerogel (0.32 g/cm$^3$) as shown in Figure 6c, and the porosity of CNF aerogel (88.5 %) was higher than the CNF/silk aerogel (73.3 %) as indicated by Figure 6d. The surface area of CNF aerogel was 47.5 m$^2$/g, which was greater than that of CNF/silk aerogel (34.2 m$^2$/g) as shown in Figure 6d. Moreover, the density, porosity, and surface area of silk aerogel made of 1% solution were 0.36 g/cm$^3$, 72.7 %, and 15.7 m$^2$/g, respectively. These results indicated that silk aerogel has higher density, but lower porosity and surface area than CNF aerogel. Addition of silk into CNF resulted to a CNF/silk aerogel that has physical property in between them.
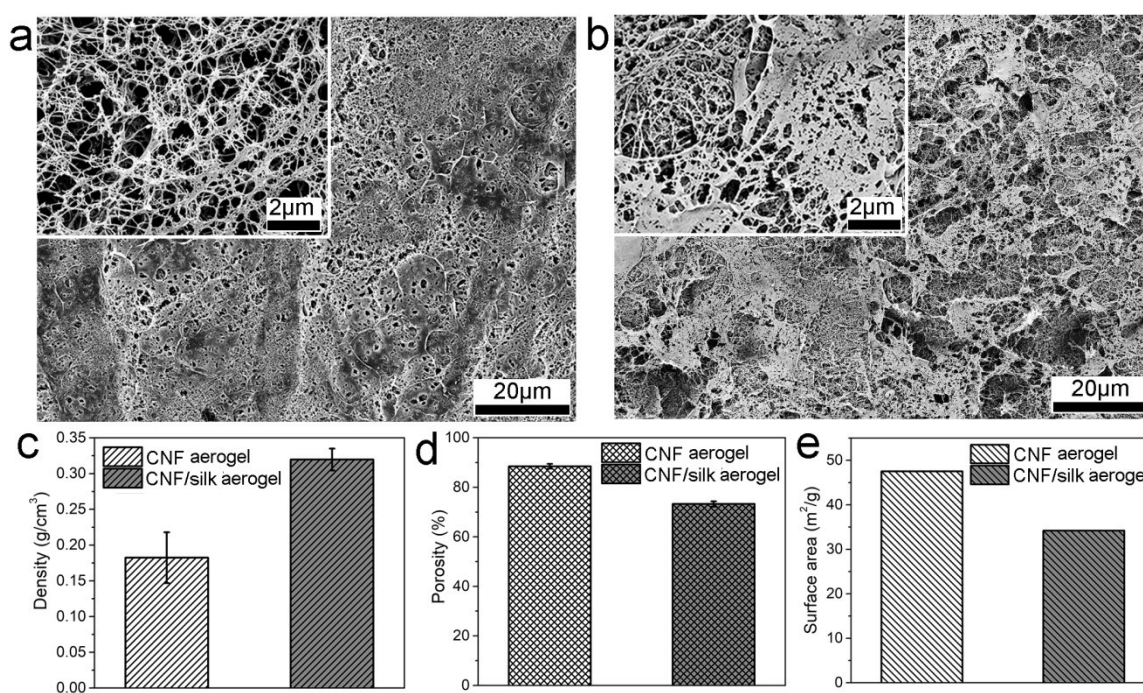


**Figure 6.** SEM images of (a) CNF aerogel membrane, and (b) CNF/silk aerogel membrane; (c) Bulk density, (b) porosity, and (c) surface area of

In terms of surface microstructure and bulk property, the CNF aerogel supposes to deliver superior triboelectric performance than the CNF/silk aerogel. However, the CNF/silk aerogel

based TENG showed higher triboelectric output than the CNF aerogel based TENG when we perform the measurements. As shown in Figure 7, the output voltage of the CNF TENG was 8.3 V, while it was 11.8 V for the CNF/silk TENG. The output current of CNF/silk TENG (1.1 μA) was also significantly greater than the CNF TENG (0.5 μA). Therefore, power of the CNF/silk TENG was 3.1 times of the CNF TENG. It was found that the output performance CNF/silk TENG could be adjusted by simply varying the ratio of silk in the hybrid aerogel. When the silk content was 10% in the hybrid aerogel, the output voltage and current were 9.2 V and 0.7 μA, respectively (Figure S6). Generally, the CNF/silk TENG outperformed the CNF TENG, although the CNF aerogel had more favorable surface morphology and higher surface area. The X-ray photoelectron spectroscopy (XPS) results (Figure S7) showed that CNF aerogel is mainly composed of C and O elements, while a significant N peak was presented in the CNF/silk aerogel indicating the amine groups on aerogel surface. The Fourier Transform Infrared Spectroscopy (FTIR) results (Figure S8) showed that amine groups appeared on the CNF/silk aerogel after addition of silk fibroin into CNF aerogel. Amine groups are electron donating groups that tend to loose electron when encounter a material that is prone to gain electron.[39, 45] Therefore, the addition of silk fibroin would lead to more charge generation during TENG operation. In this study, we have demonstrated significant positive effect of porous structure and high surface area on the improvement of the triboelectric output performance by providing more surfaces for charge generation. Here, we found that the tribopolarity of the substrate material is another critical factor that affects the output performance of TENG. Although the CNF aerogel has greater porosity and surface area than CNF/silk aerogel, the CNF/silk aerogel based TENG outperformed the CNF aerogel based TENG due to the superior tribopositivity of silk. We could conclude here that improving surface area and tribopolarity of the triboelectric material are rational approaches to improve TENG performance.
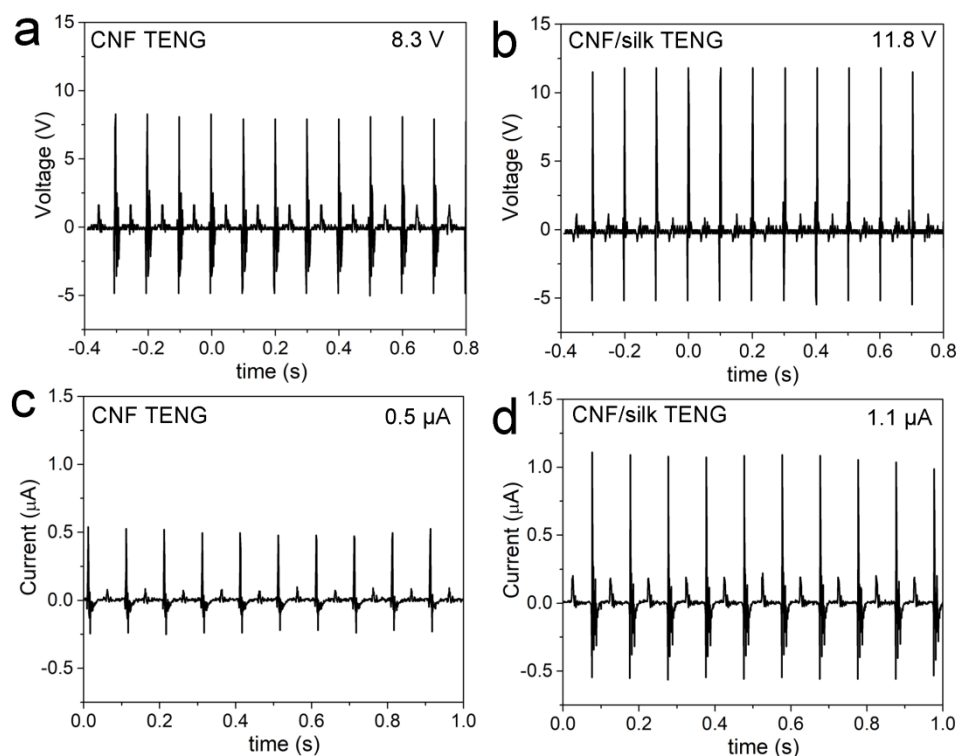
**Figure 7.** Triboelectric output voltage results of (a) CNF aerogel based TENG, and (b) CNF/silk aerogel based TENG; Triboelectric output current results of (a) CNF aerogel based TENG, and (b) CNF/silk aerogel based TENG.

## 4. Conclusion

High performance silk aerogel based TENG (STENG) was developed in this study. The STENG works in contact-separation mode and is composed of silk aerogel as the positive layer and PTFE filter paper as the negative layer. The comprehensive comparison among silk aerogels fabricated from solutions with different concentrations and raw silk fibers confirmed that the surface area had a great influence on the triboelectric performance on the porous material based STENG. HEF1 human fibroblast cell culture results proved excellent biocompatibility of raw silk fiber and silk aerogel. The STENG with the maximum surface area showed the highest output voltage and current due to the nanostructured aerogel surface and the surfaces of the inner pores, which provided more area for charge generation. The optimized STENG showed an open circuit voltage of 52.8 V and a short circuit current of 5.2

µA. A maximum power density of 0.37 W/m$^2$ was achieved when the STENG was connected to a 1 MΩ external resistor. The STENG is highly flexible and possesses high stability under different frequency and in long term. It could also be used as an energy source to power small electronics. In addition, due to the high tribopositivity of silk, silk fibroin can be used as additive material to improve the triboelectric output performance of CNF aerogel. The silk/CNF aerogel based TENG showed a 3.1 times improvement in output power compared with CNF aerogel based TENG.

**Supporting Information**

The Supporting Information is available free of charge at https://pubs.acs.org/doi/

Tensile test results of silk aerogels, cytoskeleton morphology of cells cultured for 7 days, long term output performance of STENG in 10 weeks, output voltage of STENG at various humidity, tensile test results of CNF and CNF/silk aerogels, additional output voltage data, and XPS and FTIR results of CNF, silk, and CNF/silk aerogels.

Movies about using the STENG to power LEDs, charge capacitors, and power a digital timer.

**References**

(1)   Tang, Y. F.; Zheng, Q. F.; Chen, B.; Ma, Z. Q.; Gong, S. Q. A new class of flexible nanogenerators consisting of porous aerogel films driven by mechanoradicals. *Nano Energy* **2017,** *38*, 401-411.

(2)   Li, Z.; Zheng, Q.; Wang, Z. L.; Li, Z. Nanogenerator-Based Self-Powered Sensors for Wearable and Implantable Electronics. *Research* **2020**, 8710686.

(3)   Wustenhagen, R.; Bilharz, M. Green energy market development in Germany: effective public policy and emerging customer demand. *Energ Policy* **2006,** *34* (13), 1681-1696.

(4)   Fan, F. R.; Tang, W.; Wang, Z. L. Flexible Nanogenerators for Energy Harvesting and Self-Powered Electronics. *Adv. Mater.* **2016,** *28* (22), 4283-4305.

(5)   Hu, Y. F.; Wang, Z. L. Recent progress in piezoelectric nanogenerators as a sustainable power source in self-powered systems and active sensors. *Nano Energy* **2015,** *14*, 3-14.

(6)   Wang, Z. L.; Chen, J.; Lin, L. Progress in triboelectric nanogenerators as a new energy technology and self-powered sensors. *Energ Environ Sci* **2015,** *8* (8), 2250-2282.

(7)   Zheng, Q.; Zou, Y.; Zhang, Y. L.; Liu, Z.; Shi, B. J.; Wang, X. X.; Jin, Y. M.; Ouyang, H.; Li, Z.; Wang, Z. L. Biodegradable triboelectric nanogenerator as a life-time designed implantable power source. *Science Advances* **2016,** *2* (3), e1501478.

(8)   Sun, J. Y.; Yang, A. P.; Zhao, C. C.; Liu, F.; Li, Z. Recent progress of nanogenerators acting as biomedical sensors in vivo. *Sci Bull* **2019,** *64* (18), 1336-1347.

(9)   Wang, Z. L.; Jiang, T.; Xu, L. Toward the Blue Energy Dream by Triboelectric Nanogenerator Networks. *Nano Energy* **2017,** *39*, 9-23.

(10) Zhong, X. D.; Yang, Y.; Wang, X.; Wang, Z. L. Rotating-disk-based hybridized electromagnetic-triboelectric nanogenerator for scavenging biomechanical energy as a mobile power source. *Nano Energy* **2015,** *13*, 771-780.

(11) Huang, T.; Wang, C.; Yu, H.; Wang, H. Z.; Zhang, Q. H.; Zhu, M. F. Human walking-driven wearable all-fiber triboelectric nanogenerator containing electrospun polyvinylidene fluoride piezoelectric nanofibers. *Nano Energy* **2015,** *14*, 226-235.

(12) Wang, X. F.; Niu, S. M.; Yin, Y. J.; Yi, F.; You, Z.; Wang, Z. L. Triboelectric nanogenerator based on fully enclosed rolling spherical structure for harvesting low-frequency water wave energy. *Adv. Energy Mater.* **2015,** *5* (24), 1501467.

(13) Zou, Y.; Tan, P. C.; Shi, B. J.; Ouyang, H.; Jiang, D. J.; Liu, Z.; Li, H.; Yu, M.; Wang, C.; Qu, X. C.; Zhao, L. M.; Fan, Y. B.; Wang, Z. L.; Li, Z. A bionic stretchable nanogenerator for underwater sensing and energy harvesting. *Nat Commun* **2019,** *10*, 2695.

(14) Hinchet, R.; Yoon, H. J.; Ryu, H.; Kim, M. K.; Choi, E. K.; Kim, D. S.; Kim, S. W. Transcutaneous ultrasound energy harvesting using capacitive triboelectric technology. *Science* **2019,** *365* (6452), 491-494.

(15) Fan, X.; Chen, J.; Yang, J.; Bai, P.; Li, Z. L.; Wang, Z. L. Ultrathin, Rollable, Paper-Based Triboelectric Nanogenerator for Acoustic Energy Harvesting and Self-Powered Sound Recording. *Acs Nano* **2015,** *9* (4), 4236-4243.

(16) Wu, Y.; Jing, Q. S.; Chen, J.; Bai, P.; Bai, J. J.; Zhu, G.; Su, Y. J.; Wang, Z. L. A Self-Powered Angle Measurement Sensor Based on Triboelectric Nanogenerator. *Adv. Funct. Mater.* **2015,** *25* (14), 2166-2174.

(17) Dhakar, L.; Pitchappa, P.; Tay, F. E. H.; Lee, C. An intelligent skin based self-powered finger motion sensor integrated with triboelectric nanogenerator. *Nano Energy* **2016,** *19*, 532-540.

(18) Zhang, B. B.; Chen, J.; Jin, L.; Deng, W. L.; Zhang, L.; Zhang, H. T.; Zhu, M. H.; Yang, W. Q.; Wang, Z. L. Rotating-Disk-Based Hybridized Electromagnetic-Triboelectric Nanogenerator for Sustainably Powering Wireless Traffic Volume Sensors. *Acs Nano* **2016,** *10* (6), 6241-6247.

(19) Li, Z.; Feng, H. Q.; Zheng, Q.; Li, H.; Zhao, C. C.; Ouyang, H.; Noreen, S.; Yu, M.; Su, F.; Liu, R. P.; Li, L. L.; Wang, Z. L.; Li, Z. Photothermally tunable biodegradation of implantable triboelectric nanogenerators for tissue repairing. *Nano Energy* **2018,** *54*, 390-399.

(20) Lin, Z. H.; Cheng, G.; Lee, S.; Pradel, K. C.; Wang, Z. L. Harvesting Water Drop Energy by a Sequential Contact-Electrification and Electrostatic-Induction Process. *Adv. Mater.* **2014,** *26* (27), 4690-4696.

(21) Lin, Z. H.; Cheng, G.; Lin, L.; Lee, S.; Wang, Z. L. Water-Solid Surface Contact Electrification and its Use for Harvesting Liquid-Wave Energy. *Angew Chem. Int. Edit.* **2013,** *52* (48), 12545-12549.

(22) Kim, J.; Ryu, H.; Lee, J. H.; Khan, U.; Kwak, S. S.; Yoon, H. J.; Kim, S. W. High Permittivity CaCu3Ti4O12 Particle-Induced Internal Polarization Amplification for High Performance Triboelectric Nanogenerators. *Adv. Energy Mater.* **2020,** *10* (9), 1903524.

(23) Wu, C. S.; Wang, A. C.; Ding, W. B.; Guo, H. Y.; Wang, Z. L. Triboelectric Nanogenerator: A Foundation of the Energy for the New Era. *Adv. Energy Mater.* **2019,** *9* (1), 1802906.
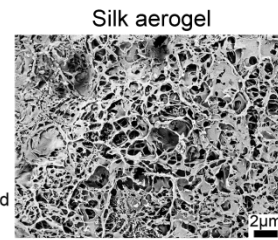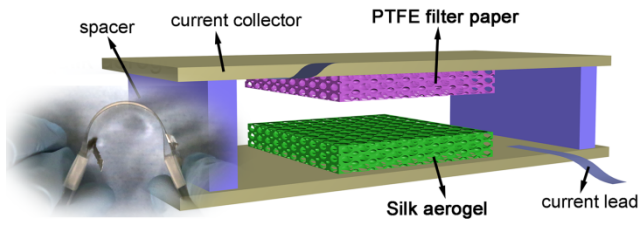
(24) Zhu, G.; Peng, B.; Chen, J.; Jing, Q. S.; Wang, Z. L. Triboelectric nanogenerators as a new energy technology: From fundamentals, devices, to applications. *Nano Energy* **2015,** *14*, 126-138.

(25) Wang, J.; Wu, C. S.; Dai, Y. J.; Zhao, Z. H.; Wang, A.; Zhang, T. J.; Wang, Z. L. Achieving ultrahigh triboelectric charge density for efficient energy harvesting. *Nat Commun* **2017,** *8*, 88.

(26) Wang, Z. L. Triboelectric nanogenerators as new energy technology for self-powered systems and as active mechanical and chemical sensors. *Acs Nano* **2013,** *7* (11), 9533-9557.

(27) Gao, X. L.; Wang, S. G.; Xu, Y. Y.; Li, H.; Zhao, H.; Pan, X. Ferulic acid and PDMS modified medical carbon materials for artificial joint prosthesis. *Plos One* **2018,** *13* (9), e0203542.

(28) Mi, H. Y.; Jing, X.; Thomsom, J. A.; Turng, L. S. Promoting endothelial cell affinity and antithrombogenicity of polytetrafluoroethylene (PTFE) by mussel-inspired modification and RGD/heparin grafting. *J. Mater. Chem. B* **2018,** *6* (21), 3475-3485.

(29) Kwak, S. S.; Kim, S. M.; Ryu, H.; Kim, J.; Khan, U.; Yoon, H. J.; Jeong, Y. H.; Kim, S. W. Butylated melamine formaldehyde as a durable and highly positive friction layer for stable, high output triboelectric nanogenerators. *Energ Environ Sci* **2019,** *12* (10), 3156-3163.

(30) Wang, R. X.; Gao, S. J.; Yang, Z.; Li, Y. L.; Chen, W. N.; Wu, B. X.; Wu, W. Engineered and Laser-Processed Chitosan Biopolymers for Sustainable and Biodegradable Triboelectric Power Generation. *Adv. Mater.* **2018,** *30* (11), 1706267.

(31) Davies, D. K. Charge generation on dielectric surfaces. *J Phys D Appl Phys* **1969,** *2* (11), 1533-1537.

(32) Li, H.; Zhao, C. C.; Wang, X. X.; Meng, J. P.; Zou, Y.; Noreen, S.; Zhao, L. M.; Liu, Z.; Ouyang, H.; Tan, P. C.; Yu, M.; Fan, Y. B.; Wang, Z. L.; Li, Z. Fully Bioabsorbable Capacitor as an Energy Storage Unit for Implantable Medical Electronics. *Adv Sci* **2019,** *6* (6), 1801625.

(33) Jiang, W.; Li, H.; Liu, Z.; Li, Z.; Tian, J. J.; Shi, B. J.; Zou, Y.; Ouyang, H.; Zhao, C. C.; Zhao, L. M.; Sun, R.; Zheng, H. R.; Fan, Y. B.; Wang, Z. L.; Li, Z. Fully Bioabsorbable Natural-Materials-Based Triboelectric Nanogenerators. *Adv. Mater.* **2018,** *30* (32), 1801895.

(34) Kim, H. J.; Kim, J. H.; Jun, K. W.; Kim, J. H.; Seung, W. C.; Kwon, O. H.; Park, J. Y.; Kim, S. W.; Oh, I. K. Silk Nanofiber-Networked Bio-Triboelectric Generator: Silk Bio-TEG. *Adv. Energy Mater.* **2016,** (6), 1502329.

(35) He, F. L.; You, X. Y.; Gong, H.; Yang, Y.; Bai, T.; Wang, W. G.; Guo, W. X.; Liu, X. Y.; Ye, M. D. Stretchable, Biocompatible, and Multifunctional Silk Fibroin-Based Hydrogels toward Wearable Strain/Pressure Sensors and Triboelectric Nanogenerators. *ACS Appl. Mater. Interfaces* **2020,** *12* (5), 6442-6450.

(36) Wen, D. L.; Liu, X.; Deng, H. T.; Sun, D. H.; Qian, H. Y.; Brugger, J.; Zhang, X. S. Printed silk-fibroin-based triboelectric nanogenerators for multi-functional wearable sensing. *Nano Energy* **2019,** *66*, 104123.

(37) Yoon, H. J.; Kim, D. H.; Seung, W.; Khan, U.; Kim, T. Y.; Kim, T.; Kim, S. W. 3D-printed biomimetic-villus structure with maximized surface area for triboelectric nanogenerator and dust filter. *Nano Energy* **2019,** *63*, 103857.

(38) Maleki, H. Recent advances in aerogels for environmental remediation applications: A review. *Chem. Eng. J.* **2016,** *300*, 98-118.

(39) Mi, H. Y.; Jing, X.; Zheng, Q.; Fang, L.; Huang, H. X.; Turng, L. S.; Gong, S. High-Performance Flexible Triboelectric Nanogenerator Based on Porous Aerogels and Electrospun Nanofibers for Energy Harvesting and Sensitive Self-Powered Sensing. *Nano Energy* **2018,** *48*, 327-336.

(40) Zheng, Q.; Fang, L.; Guo, H.; Yang, K.; Cai, Z.; Meador, M. A. B.; Gong, S. Highly porous polymer aerogel film-based triboelectric nanogenerators. *Adv. Funct. Mater.* **2018,** *28* (13), 1706365.

(41) Fu, C.; Bai, H. T.; Zhu, J. Q.; Niu, Z. H.; Wang, Y.; Li, J. N.; Yang, X. Y.; Bai, Y. S. Enhanced cell proliferation and osteogenic differentiation in electrospun PLGA/hydroxyapatite nanofibre scaffolds incorporated with graphene oxide. *Plos One* **2017,** *12* (11), e0188352.

(42) Hafner, K.; Montag, D.; Maeser, H.; Peng, C. Y.; Marcotte, W. R.; Dean, D.; Kennedy, M. S. Evaluating adhesion and alignment of dental pulp stem cells to a spider silk substrate for tissue engineering applications. *Mat Sci Eng C-Mater* **2017,** *81*, 104-112.

(43) Mi, H. Y.; Jing, X.; Meador, M. A. B.; Guo, H. Q.; Turng, L. S.; Gong, S. Q. Triboelectric Nanogenerators Made of Porous Polyamide Nanofiber Mats and Polyimide Aerogel Film: Output Optimization and Performance in Circuits. *ACS Appl. Mater. Interfaces* **2018,** *10* (36), 30596-30606.

(44)  Mi, H. Y.; Jing, X.; Cai, Z. Y.; Liu, Y. J.; Turng, L. S.; Gong, S. Q. Highly Porous Composite Aerogel based Triboelectric Nanogenerators for High Performance Energy Generation and Versatile Self-powered Sensing. *Nanoscale* **2018,** *10* (48), 23131-23140.

(45)  Lin, M. F.; Xiong, J. Q.; Wang, J. X.; Parida, K.; Lee, P. S. Core-shell nanofiber mats for tactile pressure sensor and nanogenerator applications. *Nano Energy* **2018,** *44*, 248-255.

# Table of Contents



spacer  current collector  PTFE filter paper

Silk aerogel

current lead

Silk aerogel

CNF/Silk aerogel

Surface area and output optimization